VIRGO Actuator Gain Calibration: Method and results.

Period: September 2006 - April 2007

F. Marion, B. Mours, L. Rolland (LAPP-Annecy)

D. Huet (EGO-Cascina)

VIR-005A-07

April 24, 2007

Contents

1 Introduction

The detector calibration consists in measuring its sensitivity to the gravitationnal waves (GWs). It is divided into three steps:

- calibration of the actuators used to control the mirror position, and to inject artificial calibration signals into the interferometer (ITF),
- extraction of the transfert function of the ITF,
- sensitivity estimation.

In this note, we will focus on the first step, the determination of the actuator gains and the estimation of the systematic errors. They are used in the calibration process, but also in the time domain reconstruction of h(t).

The electronic channels of the mirror actuation in the different towers are first described in section 2. The actuator gain absolute calibration methods are then explained as well as the results for the period from September 2006 to April 2007 (the Week-end Science Runs period). Relative actuator gain calibration is used to check the calibration understanding and precision as well as to extend the measurements to higher frequencies.

Some meaningfull hardware modifications history is given in the first annexe. Details of some algorithms are given in the other annexes.

2 Electronic transfer function of the coil drivers

The monitoring of the transfert function (TF) of the mirror actuators is necessary to check the comprehension of the TF and estimate some systematic errors on the calibration. Moreover, it allows to monitor and understand the hardware modifications of the coil drivers.

After a brief reminder of the position of the mirror controls, the electronic channels of the coil drivers are described for the different towers. The current measurements are shown and compared with our understanding of the electronics.

The electronic TF of the coil driver is define as the coil current over the correction signals.

2.1 Mirror controls

The mirrors of the VIRGO ITF are controlled through electromagnetic actuators, composed by a coil controled by a coil driver [5], and a magnet 'glued' to the mirror. For all towers except BS, two coils are used for the control of the mirror position along the longitudinal z-axis (the direction perpendicular to the mirror): one at the top and one at the bottom of the mirror. They are called "CoilUP" and "CoilDW". For BS, four coils are set in a diagonal way and are called "CoilUR", "CoilUL", "CoilDL" and "CoilDR" (U, R, D and L stand for up, right, down and left).

2.2 Coil driver synoptics

To control the mirror position in z, the coil drivers are converting a digital control signal (in V) into an analog current (in A). The electronic channels contain different filter, DAC and resistors depending on the mirror and of the coil. Moreover, the controls can be send through two modes:

- the high-power mode (HP) is used to acquire the lock of the ITF.
- the low-noise mode (LN) is used to control the ITF lock. The noise reduction has a counterpart: the input signal dynamic is reduced compared to the HP mode. We will see that calibration signals can not be detected in LN mode in all ITF configuration.

A coil impedence has been measured in [6]: its intrinsic inductance and resistance are $L_{coil} = 3.386 \pm 0.007\,\mathrm{mH}$ and $R_{coil} = 5.97 \pm 0.07\,\Omega$. The dispersion of both parameters in the different coils are of the order of 5% [7].

The coil driver principle is shown if Fig. 1. It can be separated into three distinct part: the digital computing in the DSP, the analog coil driver itself, and the analog sensing part. The details of the filters and gains used in the channels differ from a tower to another. A detail synoptic is shown in Fig. 2. The parameters are given in the tables 1 and 2.

Digital part: the DSP - Two digital input signals (in V) can be used to move the mirror, the calibration signal $LoopIn$[1] and the signal from the horizontal control loop. Both are digitally summed into a DSP, creating the signal $zCorr$[2] (in V). $zCorr$ is then clipped[3] to $\pm 2\,\mathrm{V}$ and sent to the HP and LN channels of both the up and down coils of the mirror (the four coils in the case of BS). For a given channel, $zCorr$ is sent to a DAC through a digital emphasis filter (zero at 3 Hz and pole at 28 Hz) and gains (G^{HP}_{DSP} or G^{LN}_{DSP}). The signal sent to the DAC of the HP channel is recorded as $zDACIn$[4] (in V).

[1] The complete names of such channels are Sc_NE_LoopIn for the NE tower for exemple.
[2] The complete names of such channels are Sc_NE_zCorr for the NE tower for exemple.
[3] The clipping is used to limit the dynamic of the DAC input signal inside its linear range.
[4] The complete names of such channels are Sc_NE_zDACIn for the NE tower for exemple.

	Digital actuation			Analog actuation					Sensing		
	emphasis		G^{HP}_{DSP}	τ_{DAC}	τ_{coil}	de-emphasis		G^{HP}_{CD}	G^{HP}_{S}	shaping	
	zero (Hz)	pole (Hz)	(V/V)	(μs)	(μs)	pole (Hz)	zero (Hz)	(A/V)	(V/A)	zero(Hz)	pole (Hz)
NE-up	-	-	1 ?	170	162	-	-	0.1947	10	3.4 *	97 *
NE-down	-	-	1 ?	170	162	-	-	0.1947	10	3.4 *	97 *
WE-up	-	-	1 ?	170	162	-	-	0.1947	10	3.4 *	97 *
WE-down	-	-	1 ?	170	162	-	-	0.1947	10	3.4 *	97 *
NI-up	2.75	24.8	1 ?	170	162?	2.75	24.8	0.1947	10	3.4 *	97 *
NI-down	2.75	24.8	1 ?	170	162?	3 *	28 *	0.1947	10	3.4 *	97 *
WI-up	2.76	25.0	1 ?	170	162?	2.75	24.9	0.1947	10	3.4 *	97 *
WI-down	2.76	25.0	1 ?	170	162?	2.78	25.3	0.1947	10	3.4 *	97 *
BS-UL	-	-	1 ?	170	??	-	-	0.1947	10	3.4 *	97 *
BS-UR	-	-	1 ?	170	??	-	-	0.1947	10	3.4 *	97 *
BS-DL	-	-	1 ?	170	??	-	-	0.1947	10	3.4 *	97 *
BS-DR	-	-	1 ?	170	??	-	-	0.1947	10	3.4 *	97 *
PR-up	-	-	10 ?	170	162?	-	-	0.1947 ?	10 ?	3.4 *?	97 *?
PR-down	-	-	10 ?	170	162?	-	-	0.1947 ?	10 ?	3.4 *?	97 *?

Table 1: ***Parameters of the coil driver channels of the different mirrors in HP mode.*** *The ticks - indicate that a component is not used in the channel. The * indicate a nominal value which has not been precisely measured.*

	Digital actuation			Analog actuation					Sensing		
	emphasis		G^{LN}_{DSP}	τ_{DAC}	τ_{coil}	de-emphasis		G^{LN}_{CD}	G^{LN}_{S}	shaping	
	zero (Hz)	pole (Hz)	(V/V)	(μs)	(μs)	pole (Hz)	zero (Hz)	(A/V)	(V/A)	zero(Hz)	pole (Hz)
NE-up	2.76	25.0	600 ?	170	0.5	2.76	25.0	0.323×10^{-3}	6 000	3.4 *	97 *
NE-down	2.71	24.5	600 ?	170	0.5	2.71	24.5	0.323×10^{-3}	6 000	3.4 *	97 *
WE-up	3.27	29.7	600 ?	170	0.5	3.27	29.7	0.323×10^{-3}	6 000	3.4 *	97 *
WE-down	3.07	27.8	600 ?	170	0.5	3.07	27.8	0.323×10^{-3}	6 000	3.4 *	97 *
NI-up	2.75	24.8	600 ?	170	0.5?	2.75	24.8	0.323×10^{-3}	6 000	3.4 *	97 *
NI-down	2.75	24.8	600 ?	170	0.5?	3 *	28 *	0.323×10^{-3}	6 000	3.4 *	97 *
WI-up	2.76	25.0	600 ?	170	0.5?	2.75	24.9	0.323×10^{-3}	6 000	3.4 *	97 *
WI-down	2.76	25.0	600 ?	170	0.5?	2.78	25.3	0.323×10^{-3}	6 000	3.4 *	97 *
BS-UL			100 ?	170	???	2.71	24.8	1.926×10^{-3}	1 000	3.4 *	97 *
BS-UR			100 ?	170	???	2.80	25.5	1.926×10^{-3}	1 000	3.4 *	97 *
BS-DL			100 ?	170	???	2.78	25.3	1.926×10^{-3}	1 000	3.4 *	97 *
BS-DR			100 ?	170	???	3.03	27.5	1.926×10^{-3}	1 000	3.4 *	97 *
PR-up	-	-	10 ?	170	162?	-	-	0.1947 ?	10 ?	3.4 *?	97 *?
PR-down	-	-	10 ?	170	162?	-	-	0.1947 ?	10 ?	3.4 *?	97 *?

Table 2: ***Parameters of the coil driver channels of the different mirrors in LN mode.*** *The * indicate a nominal value which has not been precisely measured.*

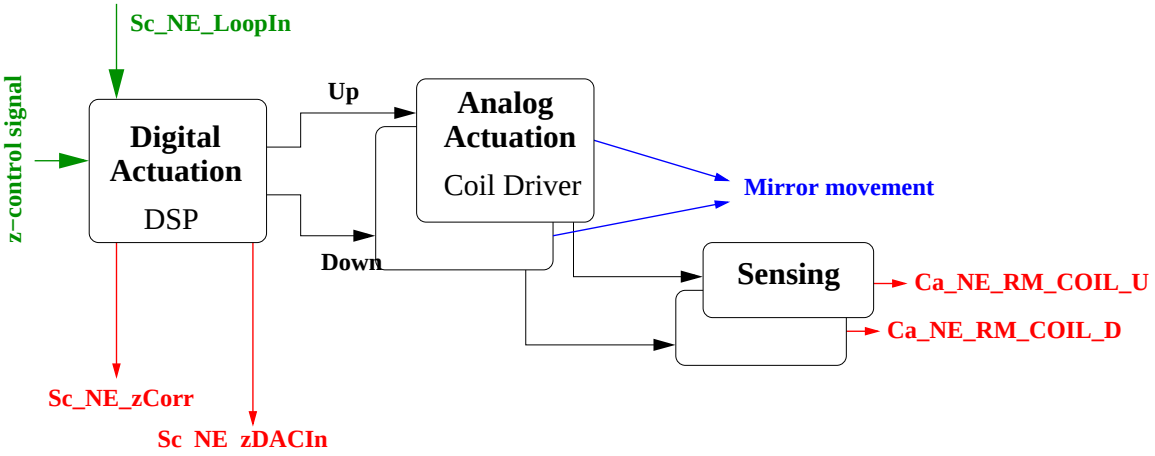

Figure 1: ***Coil driver principle***

The analogic coil driver - The DAC dynamic is ±10V. The DAC output voltage is sent to a digital de-emphasis filter[5] (pole at 3 Hz and zero at 28 Hz) and is converted into current through a serie of resistors (R_{CD}^{HP} or G_{CD}^{LN}). The current is converted by the coil into an electromagnetic force acting on the mirror magnets to move the mirror along the horizontal z direction.

The serie resistors and the coil add a delay in the TF: $\tau_{\text{coil}} = \frac{L}{R_{\text{serie}}}$, where $L = 3.4\,\text{mH}$ and R_{serie} is the sum of all serie resistors as shown in the Fig. 3. The serie resistors and the induced coil delays are given for every channels in the table 3.

From this synoptic, one can see that the same control or calibration signal is sent to the up and down coils. For the mirror longitudinal movement to be controlled properly and without inducing mirror rotation, both coils must act on the mirror magnet with similar behaviour. Thus, the TFs of both up and down channels {actuation + coil driver + coil} of a given mirror must be as close as possible.

The analogic current sensing - The current in the coil is measured through a read-out resistor (R_r^{LN} in LN and R_r^{HP} in HP). The voltage is then multiplied by a gain (G_S^{HP} or G_S^{LN}). and send through a shaping filter (zero at 3.4 Hz and pole at 97 Hz) to an ADC. The digital output voltage is measured as RM_CoilUP[6]. For a given coil, the shaping filter is the same whatever the mode is. Its zero and pole are known within 10% from the electronic components and have not been measured. The time delay induced by the ADC is compensated in the digital output signal.

Comments - The different gains, filters and resistors are set such that for a given $zCorr$ input, the current in the coil is the same both in HP and LN modes. The difference between HP and LN modes in relation to $zCorr$ is the dynamic limited by the clipping (±2V) and the DAC dynamic (±10V): in HP $zCorr$ can be as high as 2V while in LN the maximum value is $2\,V\,/\,(emph \times G_{DSP}^{LN}) \sim 2\,V\,/\,6000$, where $emph \sim 28/3 \sim 10$ is the unity gain of the emphasis filter.

In the input mirrors, the actuation de-emphasis filters, used both in HP and LN channels, are not precisely compensated in the DSP: the zero and pole of the emphasis filter are the average of the zeros and poles of the up and down channel de-emphasis filters. This induce different signals after the

[5]The de-emphasis filter poles and zeros have been measured for all mirrors. See logbook entries from September/October 2006: 13569 (NE and WE), 13582 (BS) and 13639 (NI). The WI parameters were given by Dominique Huet.

[6]The complete names of such channels are $Ca\_NE\_RM\_CoilU$ and $Ca\_NE\_RM\_CoilD$ for the NE tower for exemple. It is also measured another way as $Sc\_NE\_RM\_CoilU$ and $Sc\_NE\_RM\_CoilD$.

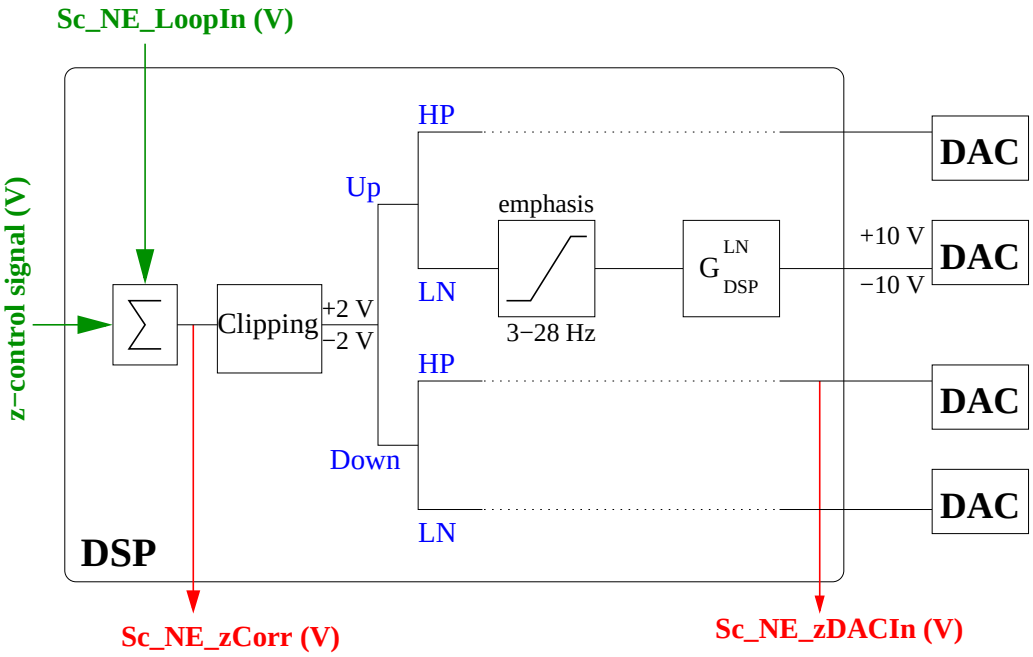

(a) Digital actuation synoptic: the DSP.

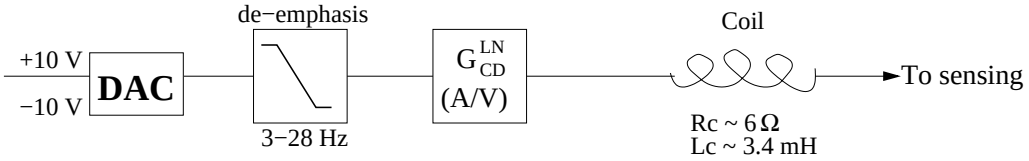

(b) Analog actuation synoptic: the coil driver.

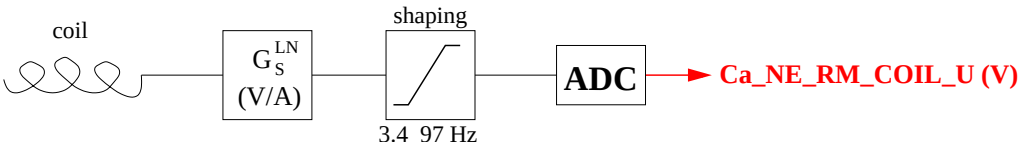

(c) Sensing synoptic.

Figure 2: ***Coil driver principle.*** *The input/output signals are called for the NE mirror. When only one channel has been drawn, the parameter names correspond to the LN channel. The different parts are described in the text and the parameter values are summarized in the tables 1 and 2.*

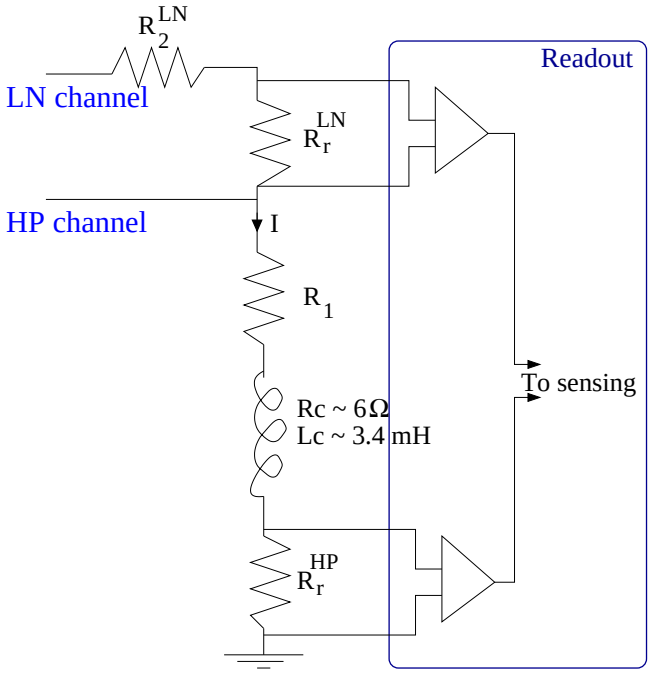

Figure 3: ***Serie resistors of a coil driver.*** *In HP mode, the current goes through R_1, including the 5 Ω of the wire resistance, R_c, the intrinsic coil resistance and R_r^{HP}, the HP sensing resistor. In LN mode, two additional resistors are added: R_2^{LN} and the LN sensing resistor R_r^{LN}. Their values are given in the table 3.*

	R_2^{LN}	R_r^{LN}	R_1 (Ω)	R_c	R_r^{HP}	$\tau_{\text{coil}^{HP}}$ (μs)	$\tau_{\text{coil}^{LN}}$ (μs)
NE	3k	3k	10+5	6	??	160	0.57
WE	3k	3k	10+5	6	??	160	0.57
NI	3k	3k	10+5?	6	??	160?	0.57?
WI	3k	3k	10+5?	6	??	160?	0.57?
BS	500	500	10+5?	6	??	160	3.2

Table 3: ***Serie resistors and induced time delays from the coils*** *of the different mirrors and modes. The serie resistors for both up and down channels of a mirror are the same (within the component specifications $\sim 10\%$). The resistors are described in the Fig. 3.*

DACs of both channels, within 10% and should affect the input actuator gain calibration. A better compensation could reduce the actuator gain calibration error.

2.3 Electronic transfert function measurements

It is possible to measure the TF of the system {actuation + coil driver + coil + sensing} as the current measured in the coil (i.e. Ca_NE_CoilU) over the input control signal (i.e. Sc_NE_zCorr). Corrections for the sensing part can then be applied in order to check the understanding of the {actuation + coil driver + coil} as used during the calibration process. For example, we define the electronic TF of the coil driver as:

$$\frac{\text{Ca\_NE\_CoilU}}{\text{Sc\_NE\_zCorr}}$$

In HP mode, a good coherence of both signals can be obtained injecting white noise as a calibration signal. Data with lower coherence but still allowing to have the global shape of the TF in data in the first steps of the lock acquisition. In LN mode, such measurements can be performed using the data in step 12 (science mode ITF) with good coherence.

2.3.1 HP TF measurements

The TFs in HP mode have been modeled from the electronics synoptics. The different components used in the model are:

- a delay τ_{DAC} from the DAC anti-alias filter ($\sim 170\mu$s),
- a delay of $\tau_{\text{coil}} = \frac{L}{R_{\text{serie}}}$ from the coil,
- a gain $G_{tot} = G_{DSP}^{HP} \times G_{CD}^{HP} \times G_{S}^{HP}$,
- a second order low pass filter with quality factor 1 and cut-off frequency 3 kHz for the coil driver,
- a shaping filter with a zero at 3.4 Hz and a pole at 97 Hz,
- an additional gain G_{add} to scale the modulus,
- an additional delay τ_{add} to match the phase.

For the end mirrors, the total delay resulting from the model without any additional delay is thus $332\,\mu$s.

HP measurements have been done on the NE tower only in November 2006[7], injecting white noise up to 1 kHz.

The Fig. 4 shows the modulus of the TFs of the NE up and down coil channels, after correction from the sensing shaping filters (nominal values). Only the frequencies were the coherence between the injected calibration signal and the coil current is higher than 95% are shown.

To match the phase shape (not shown here), the adjusted parameters G_{add} and τ_{add} are given in the table 4 for the different channels.

The shape of the modulus at high frequency is not understood yet with our current model.

[7] GPS from 848836900 to 848837090 s.

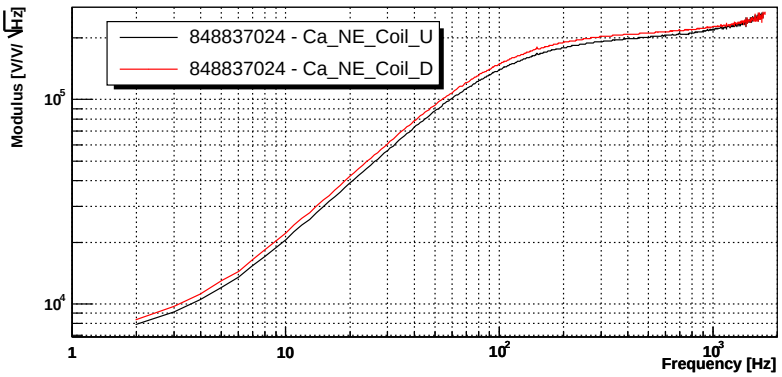

(a) Measured TF modulus.

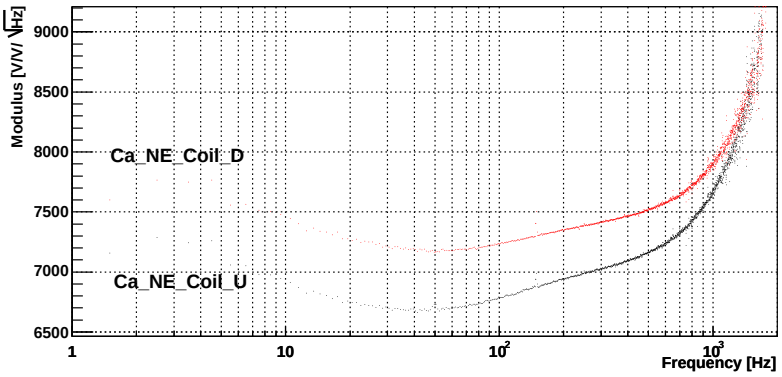

(b) TF modulus corrected from sensing filters.

Figure 4: ***TF modulus of the NE coil current over*** *zCorr* ***in HP mode.*** *(a) Measured TF modulus. (b) TF modulus after the correction for the shaping filter of the sensing (zero and pole at 3.4 and 97 Hz). Data were taken in December 2006. Only points with coherence higher than 95% are shown.*

	NE		WE		NI		WI		BS			
	U	D	U	D	U	D	U	D	UL	UR	DL	DR
G_{add}	1	1	-	-	-	-	-	-	-	-	-	-
τ_{add} (μs)	-82	-42	-	-	-	-	-	-	-	-	-	-

Table 4: ***Gain and delay parameter values added to the TF model in HP mode to the different channels.***

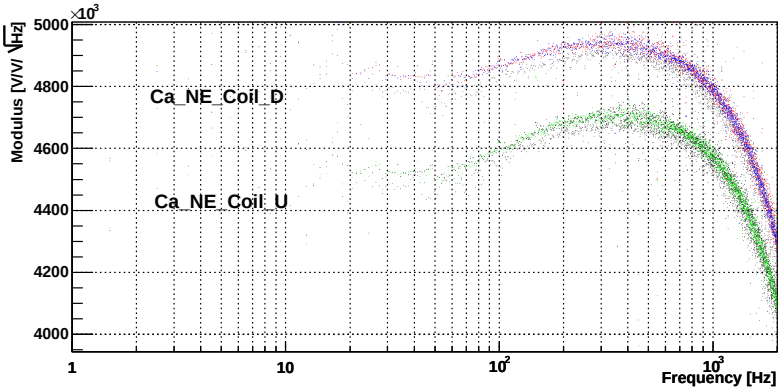

Figure 5: ***TF modulus of the NE coil current over*** *zCorr* ***in LN mode*** *for the up and down coils, after correction from the sensing shaping filters. Colors correspond to different measurements between December 2006 and March 2007. Only points with coherence higher than 95% are shown.*

2.3.2 LN TF measurements

The TFs in LN mode have been modeled from the electronics. The different components used in the model are given below. The values can be found from the table 2.

- a time delay from th DAC anti-alias filter ($\sim 170\,\mu$s),
- a time delay τ_{coil} from the coil,
- an emphasis filter,
- a de-emphasis filter,
- a total gain $G_{tot}^{LN} = G_{DSP}^{LN} \times G_{CD}^{LN} \times G_{S}^{LN}$,
- a shaping filter with a zero at 3.4 Hz and a pole at 97 Hz.
- a second order low pass filter with quality factor 1 and infinite cut-off frequency for the coil driver,
- an additional gain G_{add} to scale the modulus,
- an additional delay τ_{add} to match the phase.

The zeros and poles of the emphasis and de-emphasis filters are different from every channels and their values are given in the tables 2. The total delay resulting from the model without any additional delay is thus 170.5 μs for the end mirrors and 173.2 μs for the BS mirror.

LN measurements have been done on step 12 data from December 2006 for NE, WE and BS mirrors.

The measured modulus of the TFs, after correction from the sensing shaping filter, are shown in the Fig. 5, 6 and 7 for the different channels. Such shape represent the true coil current as function of the correction signal of the actuation, and should reflect the shape of the actuator gain ratio that one needs to calibrate (see section **??**). The adjusted parameters to match the shape of the phase G_{add} and τ_{add} are given in the table 5.

The shape of the modulus at high frequency is not understood yet with our current model.

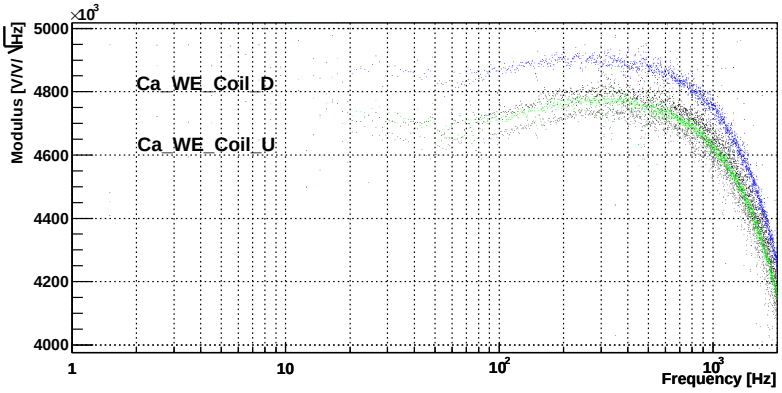

Figure 6: ***TF modulus of the WE coil current over*** *zCorr* ***in LN mode*** *for the up and down coils, after correction from the sensing shaping filters. Colors correspond to different measurements between December 2006 and March 2007. Only points with coherence higher than 95% are shown.*

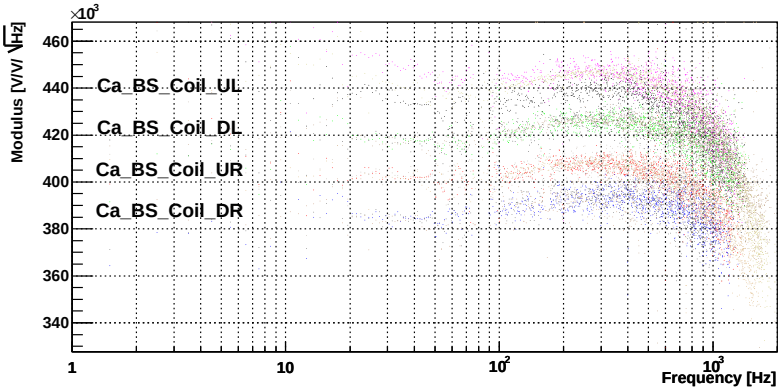

Figure 7: ***TF modulus of the BS coil current over*** *zCorr* ***in BS mode*** *for the four coils, after correction from the sensing shaping filters. Colors correspond to different measurements between December 2006 and March 2007. Only points with coherence higher than 95% are shown.*

	NE		WE		BS			
	U	D	U	D	UL	UR	DL	DR
G_{add}	1	1	1	1	1	1	1	1
τ_{add} (μs)	120	170	120	170	80	80	80	80

Table 5: ***Gain and delay parameter values added to the TF model in LN mode to the different channels.***

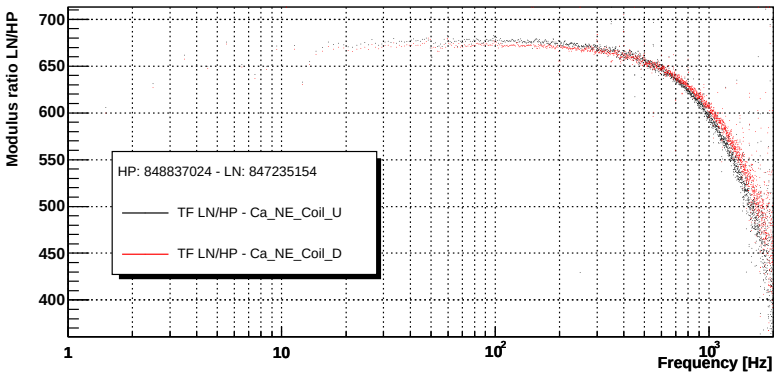

Figure 8: ***Ratio of the LN to HP TF modulus of the NE coil current over*** *zCorr for the up and down coils. Data are from December 2006. Only points with coherence higher than 85% in both LN and HP channels are shown.*

2.3.3 Ratio of the LN to HP electronics actuation TFs

The ratio of the LN to HP electronics actuation TFs contributes to the ratio of the actuator gain in LN and in HP. It should even be the only contribution to the gain ratio, thus allowing to transfer the HP gain to the LN gain used during scientific runs.

The ratio of the LN to HP electronics actuation TFs for the NE tower is shown in Fig. 8. The predicted ratio given the electronics The ratio at low frequency is flat around 660 It varies by 8% below 1 kHz and up to 30% below 2 kHz. Still need to comment on this.

2.3.4 Additionnal measurements to be performed

The TFs should be regularly measured and checked for all the towers in LN and HP modes. Step 12 data can be used to get the TFs of the NE, WE and BS channels in LN mode[8]. Specific white noise injections should be done to mesure the TFs of the input mirror actuations.

To measure the TFs in HP mode, two ways are possible[9]: one can do specific white noise injections (in the range 1 Hz to 1 kHz), or compute the TF in the first steps of the locking aquisition (in the range 1 to 200 Hz), before the suspensions are switched to LN mode.

[8] A VEGA script has been created in the script/ directory of the module Cali: ComputeActuationTF.C

[9] In principle, it could also be possible to compute the TF at the frequencies used to measure the actuation gain in free swinging Michelson (see section FreeMichelson). However, the ADC dynamic of the sensing part is too low: the injected line amplitude saturate the read-out electronics.

3 Actuator gain calibration

The complete system used for the calibration line injection is {actuation + coil driver + coil + mirror}. The mechanical response of the suspended mirror has been measured [3] and is described by a pendulum with a resonnance at $f_0 = 0.6$ Hz:

$$M(f) \propto \left[-\left(\frac{f}{f_0}\right)^2 + \frac{\mathrm{i}}{Q}\frac{f}{f_0} + 1\right]^{-1}$$

where the quality factor Q is larger than 500.

One can measured the TF of the mirror diplacement as function of the injected calibration signal, and correct it from the mechanical response of the mirror. One should then find the flat TF described in the previous section. This process permits to measure the absolute actuator gain, in m/V. Such measurements can be done using free swinging Michelson configuration, but only in HP mode. As the tower suspension are in LN mode during the science mode runs, the interesing values are the actuator gains in LN mode. They can be computed using locked cavity data and the previously measured HP actuator gain.

3.1 Theoretical estimation of the actuator gains

The actuator gain can be estimated theoretically from the conversion factors of the coil driver electronic TF (A/V), the current-force conversion factor (N/A) and the response of the mirror to the applied force.

From the model described in section 2.3, the coil driver electronic conversion factor $\gamma = G_{DSP} \times G_{CD}$ is 0.1947 A/V in HP mode as well as in LN mode (within $\sim 10\%$). The current-force conversion factor [6] α is 10.7 mN/A.

The input and end mirrors have a mass $M = 22$ kg and can be modelised by a simple pendulum with length $l = 0.7$ m. Their longitudinal movement is controlled by two coils.

The actuator gain is thus:

$$G^{\mathrm{actuator}} = \frac{\delta x}{V} = \frac{2F}{M \times \frac{g}{l}} = \frac{2\gamma\alpha}{M \times \frac{\mathrm{g}}{l}}$$

where $\mathrm{g} = 9.81\,\mathrm{m.s}^{-2}$.

With the numbers given above, the actuator gain for the arm mirrors in both HP and LN modes is found to be:

$$G^{\mathrm{actuator}} = 13.5\,\mu\mathrm{m/V} \quad (1)$$

For the BS mirror, the conversion factor is $\gamma = 0.1947$ A/V, the mass $M_{BS} = 5$ kg and the longitudinal movement is controled through four coils. However, for a diplacement dl of BS along its longitudinal axis, the movement along one arm axis is $dl \times \cos(45°) = dl \times \sqrt{2}/2$. As the displacement is the same on both arms, the effective displacement of the mirror is $dl \times \sqrt{2}$. The effective actuator gain is thus estimated to:

$$G_{BS}^{\mathrm{actuator}} = \sqrt{2} \times 119\,\mu\mathrm{m/V} = 170\,\mu\mathrm{m/V} \quad (2)$$

We note an overstimation of this estamation by a factor 2 compared to the measurements. Checks in the model should explain this...

3.2 Free swinging Michelson measurements: gain in high power mode

In the free Michelson configuration of the ITF, the actuator gain can be measured at different frequencies injected calibration lines. Only one mirror of each arm can be calibrated at once, using different configuration:

- Long Michelson to calibrate NE and WE gains,
- Short Michelson to calibrate NI and WI gains,
- Asymmetric Michelson to calibrate NE and WI or NI and WE gains.

The BS gain can be computed in all configurations. The PR gain cannot be calibrated in free Michelson configuration.

In order to do the calibration, the mirror relative displacement ΔL must be computed. Then the TF of the ΔL over the injected calibration signal $zCorr$ gives the tower actuator gain at the injected frequency.

After the description of the data configuration, we describe the calculation of the mirror displacement ΔL using the dark fringe signals. Then, the results and issues obtained during the November 2006 calibration shift are given.

3.2.1 Data configuration

The data are taken in 4 different free Michelson configurations in order to measure the actuator gains for the five mirrors NE, WE, NI, WI and BS. To perform this, the PR mirror and some arm mirrors are misaligned:

- Long Michelson: both input mirrors misaligned.
- Short Michelson: both end mirrors misaligned.
- Asymmetric Michelson (2 possibilities): one input mirror and the other arm's end mirror misaligned.

The input, end and PR mirrors are misaligned horizontally (changing the θ_y angle) by -350, -150 and $-200\,\mu$rad respectively.

In order to have free Michelson configurations, some mirror controls must not be used for this data. The lines are injected through DSPs where the $Cali$ variable must be set to 1 to take them into account.

- mirror longitudinal local controls (z-dampers) switched off,
- re-allocation of the low frequency (< 40 Hz) control signals to the marionnette switched off,
- mirror suspensions in HP mode (in LN mode, the dynamic is too low due the use of the emphasis-filters and the gain G^{LN}_{DSP} of 600. Thus the injected lines are not visible).

3.2.2 Mirror displacement calculation

The measurement of the displacement of the mirror is based on a non-linear reconstruction of the differential mode of the ITF, using the laser wavelength as length reference. In open loop, the direct and demodulated dark fringe signals (PR_B1p and PR_B1, DC, ACp and ACq) depends on the phase difference $\Delta\Phi$ between both interfering beams:

$$V_{B1p\_DC} = B\,(1 - C\,\cos\Delta\Phi) \quad (3)$$

$$V_{B1p\_ACq} = A\,\sin\Delta\Phi \quad (4)$$

$$V_{B1p\_ACp} = A\,\sin\left(\Delta\Phi + \pi/2\right) \quad (5)$$

where A and B are proportional to the laser power and C is the ITF contrast. Two methods are used to estimate $\Delta\Phi$ from the DC and one AC signals. The differential mirror displacement is then estimated as:

$$\Delta L = \frac{\lambda}{4\pi}\Delta\Phi$$

where $\lambda = 1.064\,\mu$m is the laser wavelength.

The first method, called $MinMax$ in the following, is described in [2, 4]. The A, B and C parameters are estimated from the dark fringe signals and updated regularly:

$$A = \frac{V^{max}_{B1p\_ACq} - V^{min}_{B1p\_ACq}}{2} \quad (6)$$

$$B = < B_{B1p\_DC} > \quad (7)$$

$$C = \frac{V^{max}_{B1p\_DC} - V^{min}_{B1p\_DC}}{2B} \quad (8)$$

and then $\Delta\Phi$ is derived from:

$$\cos\Delta\Phi = -\frac{V_{B1p\_DC}}{B \times C} \quad (9)$$

$$\sin\Delta\Phi = \frac{V_{B1p\_ACq}}{A} \quad (10)$$

Details of the algorithms are described in annexe B.

The second method, called *Ellipse* in the following, is based on an ellipse fitting [8] of the two-dimension plot of the AC vs DC signals. The fit is regularly processed and gives the ellipse centre position (theoretically $(B, 0)$) and the axis widths (theoretically $(-BC, A)$). $\Delta\Phi$ can then be deduced directly. The details of the algorithms are described in annexe C.

Comparison of ΔL estimations on simulated data - Simulations were done to compare and estimate the systematics of the different methods. A signal $\Delta\Phi$ is simulated as function of time as the sum of sinusoides. A and B are proportional to a simulated laser power so that their values are close to the real ones. C is set to a possible ITF contrast value. Gaussian noise can be added to the values of $\Delta\Phi$, the laser power and C. The signals are sample at a rate of 20 kHz and saved into frames that can be read as real data from VIRGO. The ΔL estimation algorithms are then applied to the simulated data.

An exemple of simulated ΔL as function of time and FFT are shown in figure 9, as well as the reconstructed values from both methods. From the time evolution, one can see that the relative displacement of the mirror are globally well reconstructed. The FFTs show that the *Ellipse* method has a lower noise level.

The important parameter to reconstruct is the line amplitude in the FFT. The relative amplitude differences of the reconstructed ΔL at the seven simulated injection frequencies are given for both $MinMax$ and *Ellipse* method in the table 6. Both methods reconstruct the line amplitudes within 3%. One should perform the TF of the reconstructed ΔL over the simulated one in order to get the resolution independently of the reconstruction noise.

Comparison of ΔL estimations on real data - After selection of data with good quality, the ΔL has been reconstructed by four different means (using the ACq or the ACp signals $B1p$, and both methods $MinMax$ or *Ellipse*). The figure 10 show the time evolution and FFTs of the four reconstructed values. On these data, the noise level was higher on Pr_B1p_ACq than on Pr_B1p_ACp which explains the fact that the ACq FFTs have larger noise than the ACp ones. This might not be always the case and needs to be checked for every calibration data. The comparison of

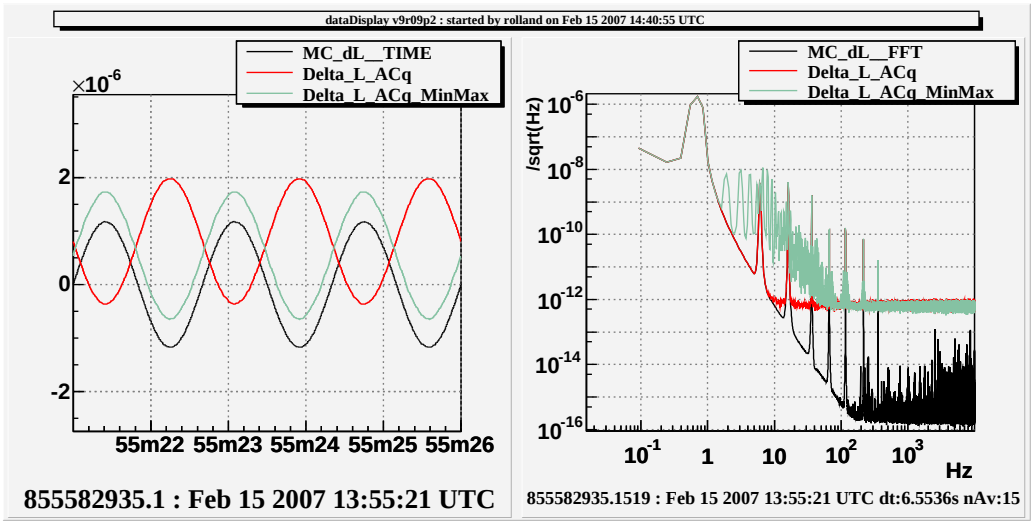

Figure 9: ΔL ***as function of time and FFT.*** *The reconstructed values from MinMax and Ellipse methods are superpose to the simulated data. The simulated* $\Delta\Phi$ *is the sum of lines at* 0.6, 6, 16, 36, 66, 116, 216 *and* 356 *Hz with respective amplitudes (in units of* $2\pi \times 10^{-3}$*)* 2.2×10^3, 5, 5, 2, 0.2, 0.2, 0.1 *and* 0.02. *The power and contrast are assumed constant as function of time, resulting in* A, B *and* C *value of the order of* 2×10^{-5}, 4×10^{-4} *and* 0.98 *respectively. Gaussian noise is added to the laser power and contrast at the level of* 0.1%. *The noise is seen on the simulated* $B1p\_DC$ *and* $B1p\_AC$ *signals, but not on the simulated* $\Delta\Phi$.

Frequency (Hz)	6	16	36	66	116	216	356
$\frac{\Delta L^{MinMax} - \Delta L^{Simu}}{\Delta L^{Simu}}$ (%)	-	3.6	3.4	3.6	3.3	3.4	3.1
$\frac{\Delta L^{Ellipse} - \Delta L^{Simu}}{\Delta L^{Simu}}$ (%)	0	0	0	0	-0.1	0.1	-0.1

Table 6: ***Relative difference between the reconstructed line amplitude to the simulated one*** *is given in % for both MinMax and Ellipse methods for the 7 injected lines.*

Frequency (Hz)	7	17	37	67	117	217	357
$\frac{\Delta L^{MinMax} - \Delta L^{Ellipse}}{\Delta L^{Ellipse}}$ (%)	0.6	2.2	1.2	-0.6	0.3	-0.3	-0.5

Table 7: ***Relative difference between the reconstructed line amplitudes*** *using both MinMax and Ellipse methods for the 7 injected lines on data at GPS 848217700.*

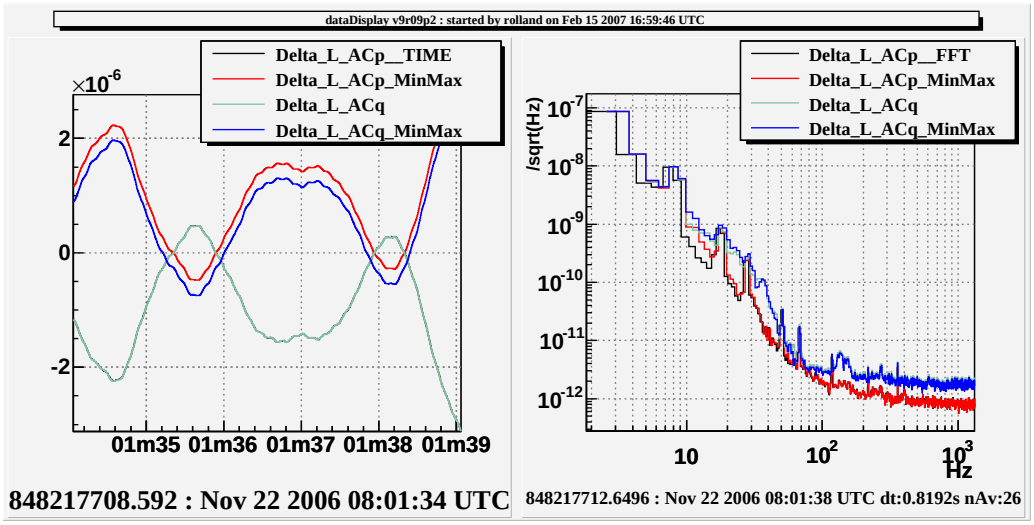

Figure 10: ***Reconstructed*** ΔL ***vs time and FFTs on real data.*** ΔL *was reconstructed using both MinMax and Ellipse methods, and both* Pr_B1p_ACp *and* Pr_B1p_ACq *signals.*

the two reconstructions from Pr_B1p_ACp shows that the both method are simimar concerning the noise level, execept around 10 Hz where the *Ellipse* method adds a factor 2 less noise.

For the reconstruction using Pr_B1p_ACp, the time evolution of the parameters used in the *MinMax* and *Ellipse* methods are shown in the figures 11 and 12. The comparison of the data ellipse from Pr_B1p_ACp vs Pr_B1p_DC and the parameter values indicate that their are correctly reconstructed and they have slow variations. During 150 s of data, the distribution of the different parameters are stable within 4% for the $MinMax$ parameters and within 0.3% for the ellipse parameters.

The relative differences of the reconstructed line amplitudes for both methods using the signal Pr_B1p_ACp are given in the table 7. Both methods agree within less than 3%, in agreement with the simulation checks.

3.2.3 Data quality selection

Here are summarized some ideas to check for data quality. They are not yet implemented in the code:

- constant power mode vs time
- the zDampers are switched off: $|zCorr - zLoopIn| < 1\% \, zLoopIn$
- the marionnette reallocation is switched off: $zM = 0$
- the injected line amplitudes are constant (constant zLoopIn FFT amplitudes vs time)
- the injected lines do not saturate the actuation electronics

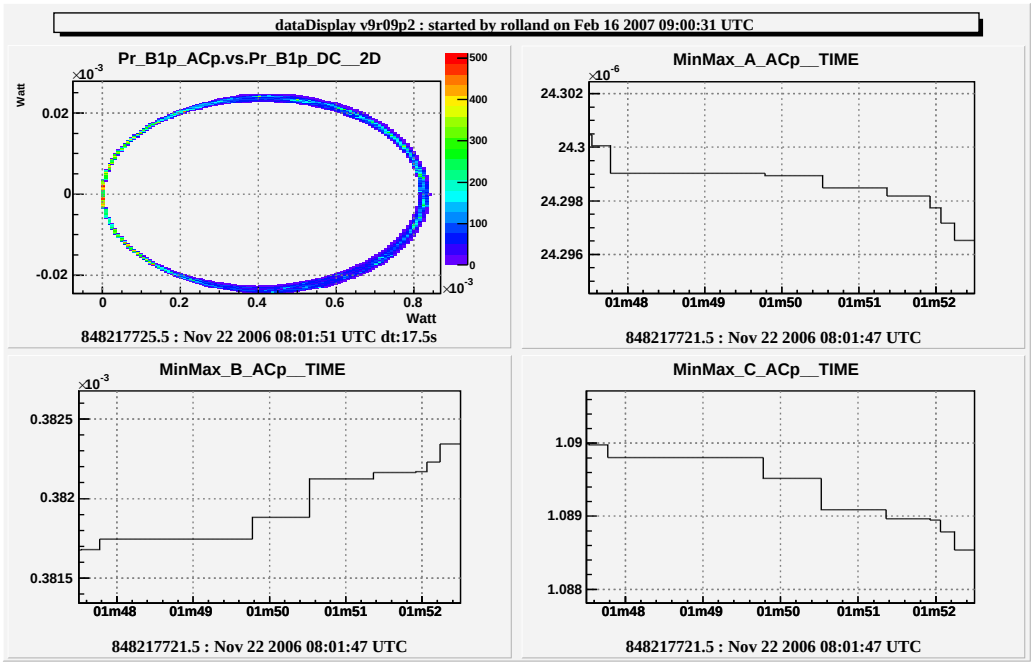

Figure 11: ***Time evolution of the three parameters used in the*** *MinMax* ***method on 5 s of real data.*** *The two-dimension plot of* Pr_B1p_ACp *vs* Pr_B1p_DC *is given for reference. The reconstructed parameters are the averaged values of* A*,* B *and* C*.*

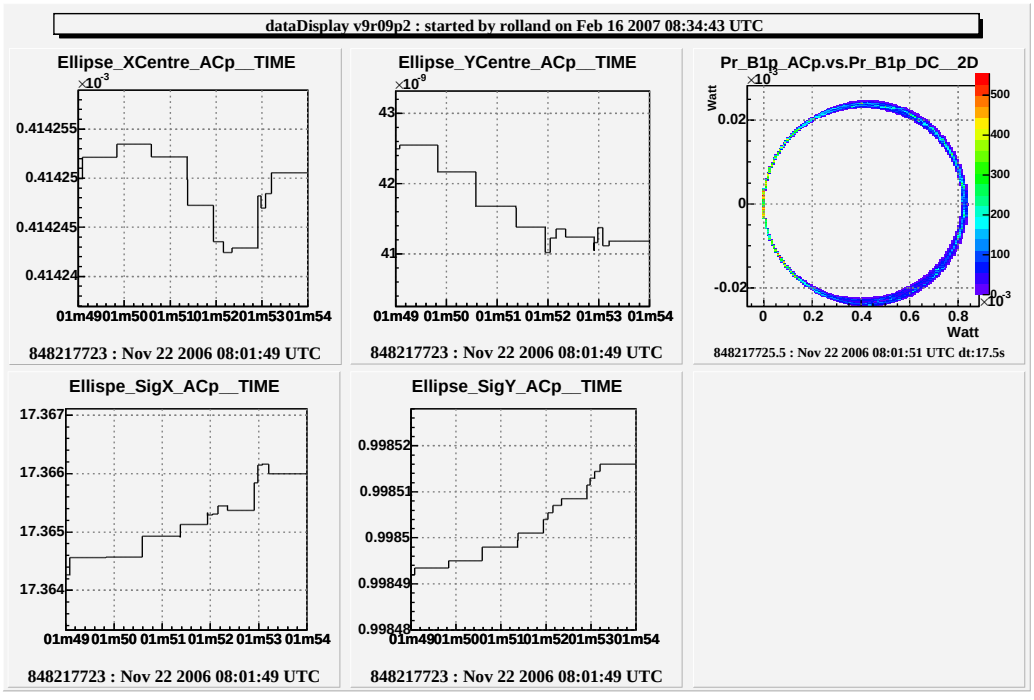

Figure 12: ***Time evolution of the reconstructed ellipse parameters in the*** *Ellipse* ***method on 5 s of real data.*** *The ellipse from* Pr_B1p_ACp *vs* Pr_B1p_DC *is also given for reference. The reconstructed parameters are the position of the centre of the ellipse (*$Ellipse\_XCentre\_ACp$ *and* $Ellipse\_YCentre\_ACp$*), and the normalized axis widths (*$Ellipse\_SigX\_ACp$ *and* $Ellipse\_SigY\_ACp$*).*

Tower	Gain (μm/V)	Pole (Hz)	Zero (Hz)	Delay (μs)
NE	12.1	100	125	480
WE	10.9	100	125	480
NI	13.7	100	125	480
WI	12.0	100	125	460
BS	78.0	–	–	450

Table 8: ***Adjusted parameters of the actuation TF as function of frequency in HP mode*** *for the input, end and BS mirrors on the calibration data from March 2007. Errors on the matched parameters are estimated to 5%.*

- the alignement is not too noisy, which results in a stable and thin ellipse AC vs DC:
  - AC: mean <1% max
  - DCmin∼0
  - DCmax>10 ACmax

3.2.4 Measurements in long and short Michelson configurations

The results shown below were obtain on data from March, 7th 2007 (logbook entries 15496 and 15626). Measurements in short and asymmetric Micheslon were performed in order to measure the actuator gains of the NE, WE, NI, WI and BS mirrors in HP mode. Different datasets were obtained with different line frequencies and amplitudes.

The noise level of the reconstructed ΔL depends on the ITF configuration and on the AC signal used. In the short Michelson configuration, the less noisy ΔL is computed using Pr_B1p_ACp, while in the asymmetric configurations, the use of Pr_B1p_ACq is better.

The figures 13, 14, 15, 16 and 17 show the measured gain and phase of the actuation TF at the injected lines frequencies, only for points with coherence higher than 99.9% between $zCorr$ and ΔL. The error bars were estimated from the empiric formulae from [4]:

$$\frac{\mathrm{d}M}{M} = \alpha \sqrt{\frac{1-C}{C}} \frac{1}{\sqrt{n_{call}}} \tag{11}$$

$$\mathrm{d}P = \beta \sqrt{\frac{1-C}{C}} \frac{1}{\sqrt{n_{call}}} \tag{12}$$

where M and P are the modulus and the phase of the TF respectively, C the coherence, n_{call} the number of averages performed on the TF, α and β two constants respectively estimated to 0.85 and 0.88.

These measurements confirm the TF dependency with the frequency on the end and input mirrors (discovered during the November 2006 calibration shift, see logbook entry 14195) while very low frequency dependence is seen on the BS actuation. The TF has been parametrized with a pole and a zero to match the modulus dependence. A delay has been also added to the phase. On the phase, different offsets are measured within $(-90, 0, 90, 180°)$ depending on the ITF configuration The table 8 summarizes the fitted parameters for the different towers and the different datasets. The parametrisation does not match the measurements above $\sim$ 300 Hs. However, using such a parametrisation might overestimate the gain value and thus is conservative concerning the estimated sensitivity.

3.3 Actuation gain transfert from HP to LN mode

The actuator gain transfert from HP to LN mode can be done with specific data allowing to compare the gain from a tower in LN mode to the known gain of a tower in HP mode:

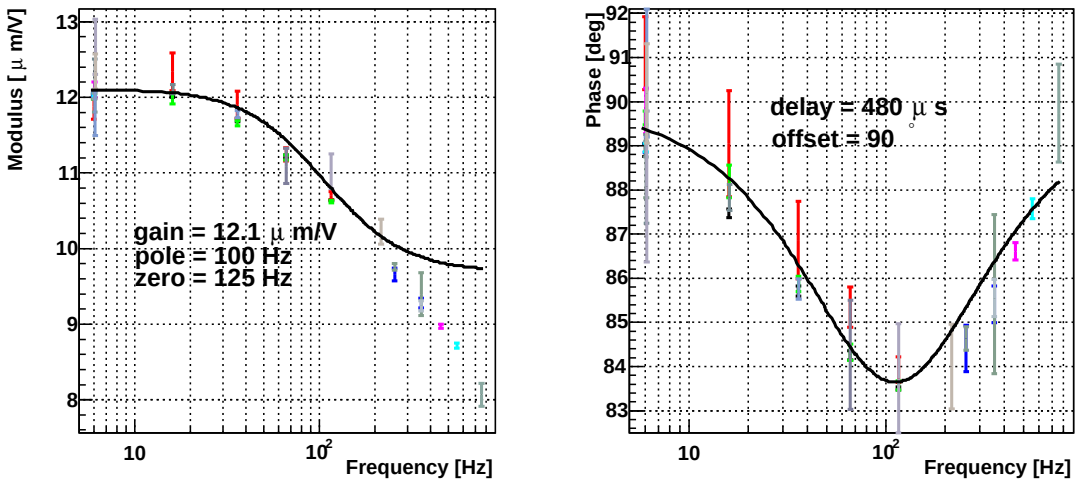

Figure 13: ***Actuator gain of NE in HP mode.*** *All points have coherence higher than 99%. The different colors represent different datasets.*

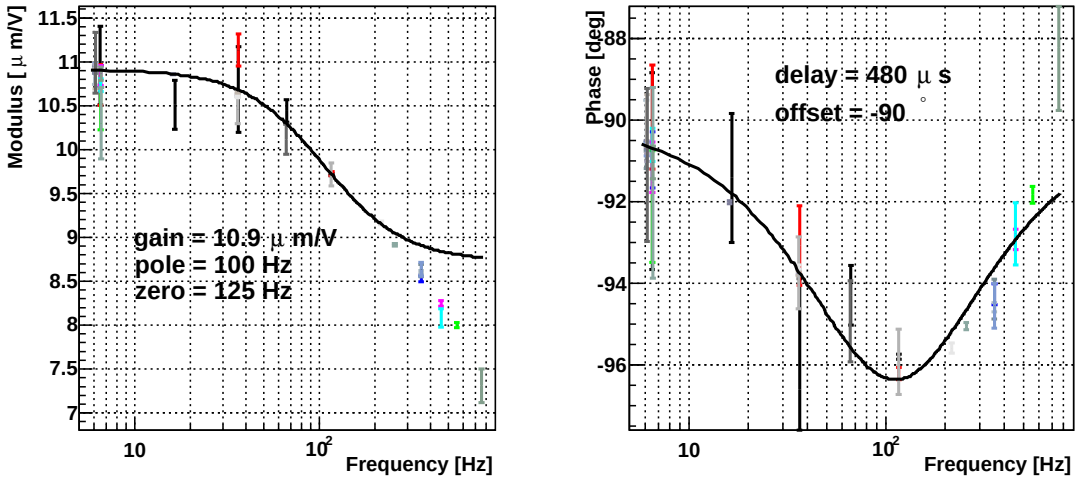

Figure 14: ***Actuator gain of WE in HP mode.*** *All points have coherence higher than 99%. The different colors represent different datasets.*

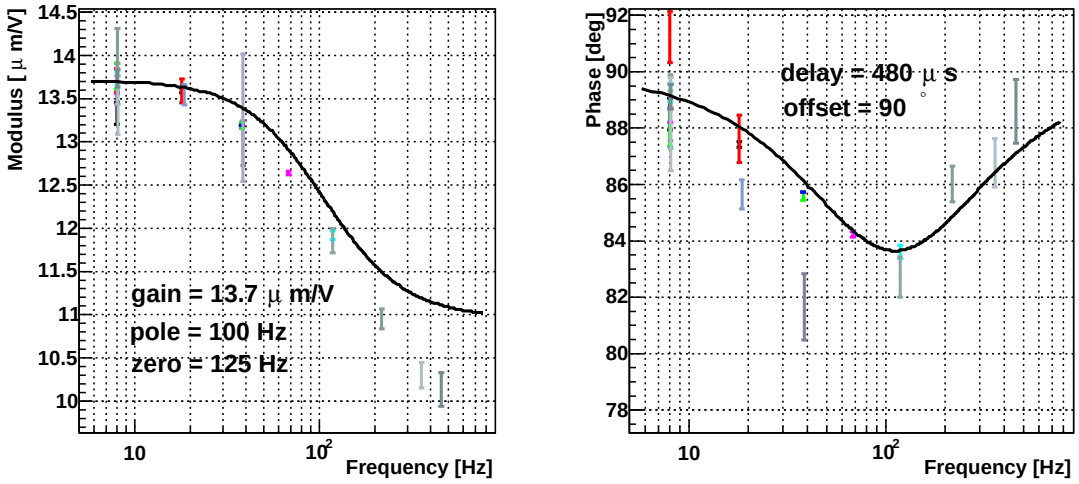

Figure 15: ***Actuator gain of NI in HP mode.*** *All points have coherence higher than 99%. The different colors represent different datasets.*

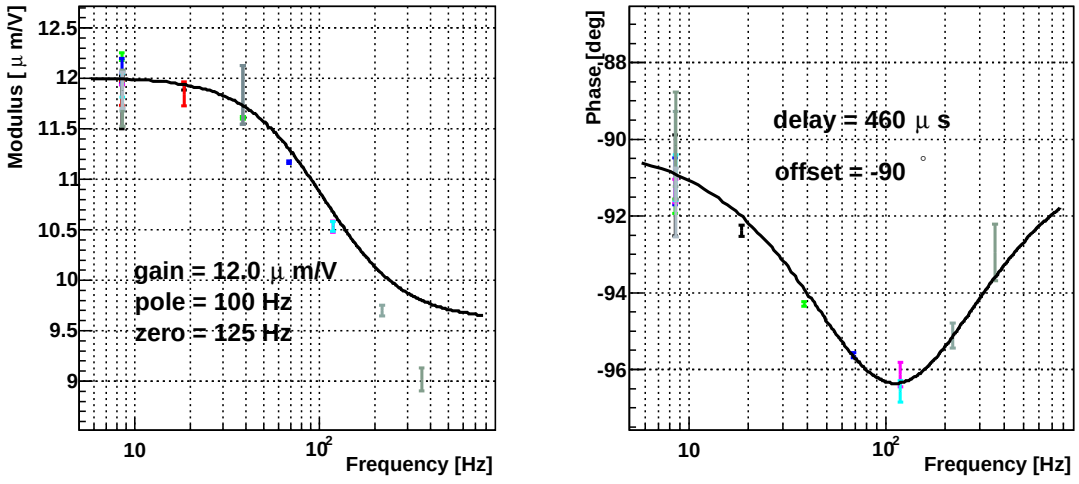

Figure 16: ***Actuator gain of WI in HP mode.*** *All points have coherence higher than 99%. The different colors represent different datasets.*

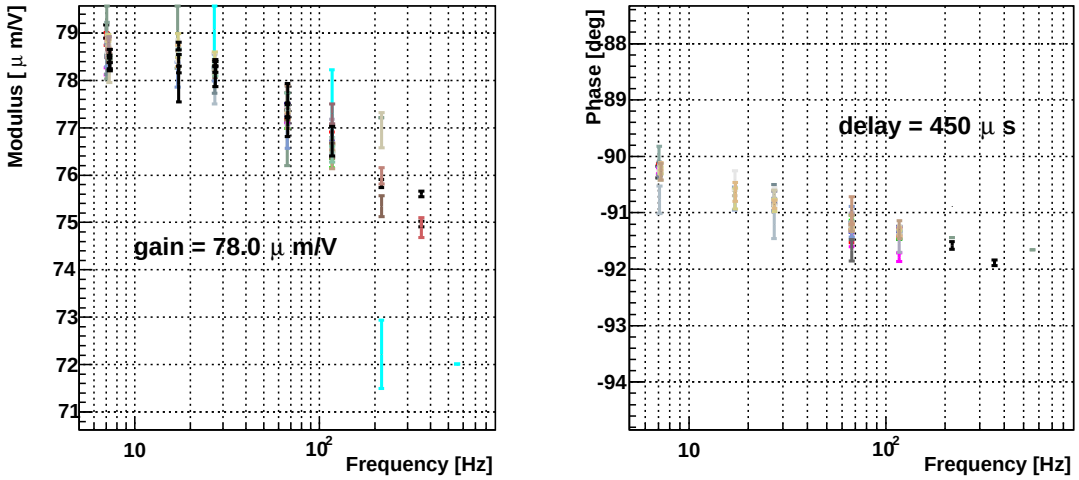

Figure 17: ***Actuator gain of BS in HP mode.*** *All points have coherence higher than 99.99%. The different colors represent different datasets.*

- transfert from a mirror to another using a locked cavity with one mirror in HP and one mirror in LN mode. Couple of lines are injected into both mirrors (frequency within 0.5 Hz from each other same amplitude). The line amplitude ratio (corrected from the pendulum response at both frequencies) is equal to the ratio of the actuator gains at this frequency. In this configuration, the ITF might not be sensitive to the lines injected to fulfill the low LN dynamics. This still has to be checked.

- transfert within a mirror using data in step 10 of the locking acquisition. The suspension mode is switched after some minutes. For a line injected on the mirror, one can compute the TF of the dark fringe signal Pr_B1_ACp to the correction signal Sc_NE_zCorr, once in LN mode, once in HP mode. Assuming a constant optical gain of the cavity between both datasets, the ratio of both TFs at the injected frequency gives the ratio of the gain.

The second method can also be performed with the fully locked ITF (step 12), switching the input towers from LN to HP only. This was done on March 7th, 2007 [10]. 19 lines were injected on the mirrors from 5 to 600 Hz. The Fig. **??** The **preliminary** Fig. **??** and **??** show the LN to HP ratio as function of frequency for the different injected lines, where the coherence of the dark fringe to the correction signal is higher than 90% in both datasets. The coherence is close to 99% at every injected frequencies except between 60 and 150 Hz where the HP coherence is around 95%. The errors seem underestimated.

For the NI actuation, the LN to HP ratio below 100 Hz is equal to 1 within less than 5%, and is close to 1.1 between 300 and 600 Hz. For the WI actuation, larger variations are seen.

3.4 Actuation gains in LN mode

The sensitivity estimation and the h-reconstruction are done with locked ITF, with all suspensions in LN mode. The LN gain can be estimated from the HP gain and the LN to HP ratio. However, the gain ratio are only preliminary results and were not measured for the end mirrors and BS. From the

[10] 857288004-85728740: all suspensions in LN mode. 857288950-857289255: input mirror suspensions in HP mode.

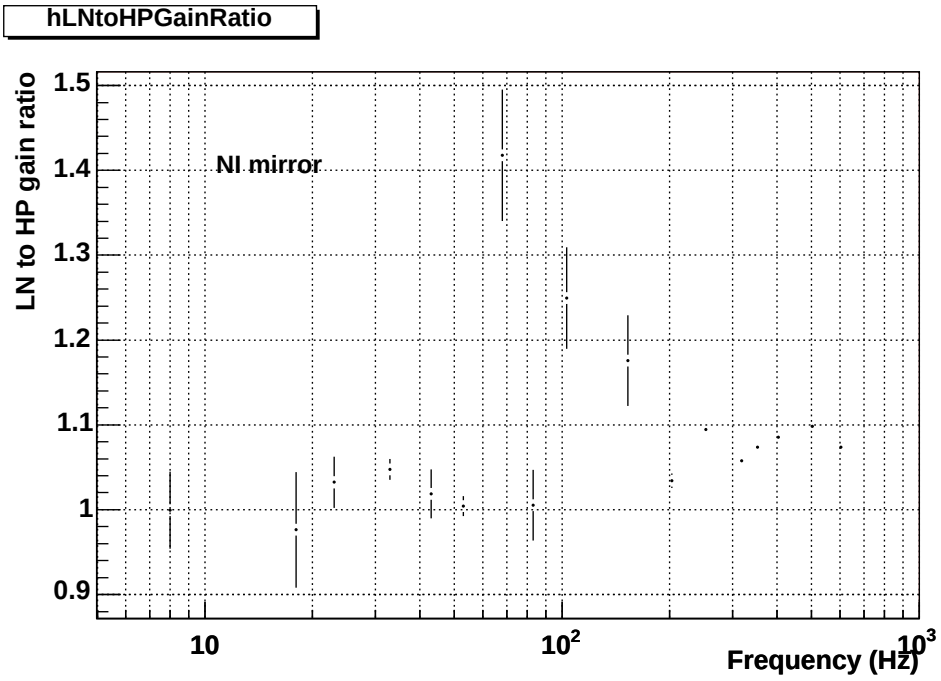

(a) NI suspensions.

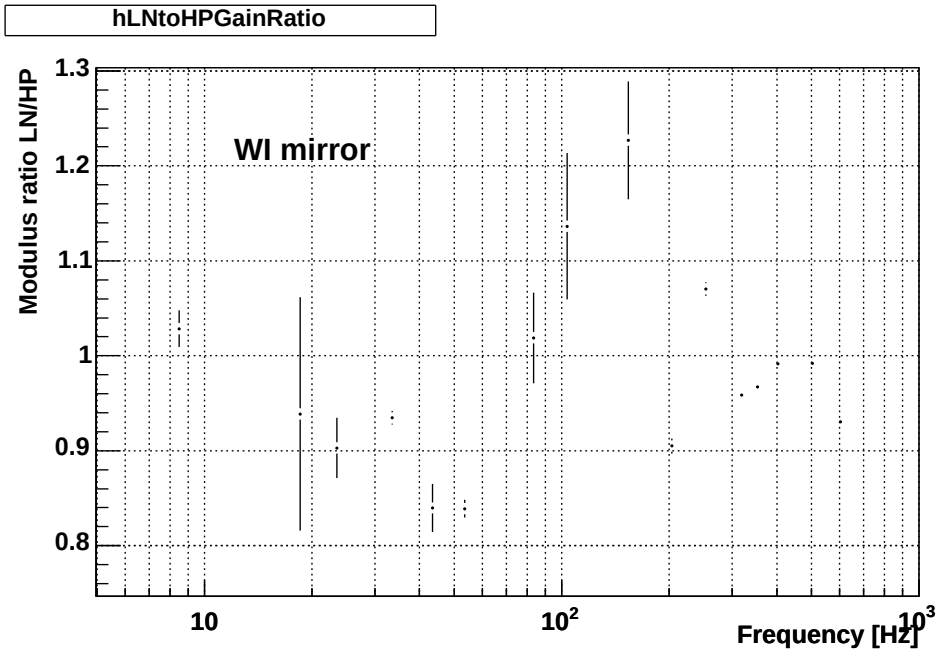

(b) WI suspensions.

Figure 18: ***Actuator gain ratio LN to HP for the input mirrors*** *as function of the frequency. Only the injected frequencies were the coherences of both TFs were higher than 90% are shown.*

Tower	Gain (μm/V)	Pole (Hz)	Zero (Hz)
NE	12.7	100	125
WE	11.5	100	125
NI	14.4	100	125
WI	12.6	100	125

Table 9: ***Parametrization of the actuation TF as function of frequency in LN mode*** *for the end and input mirrors.*

input gain ratio, we can assume that the LN gain are not higher by more than 5% than the HP gain at low frequency. At higher energy, the parametrisation with a pole and a zero already gives conservative gain values. More precise values will be measured before the scientific run. We thus presently use the values given in the table 9 for the sensitivity and reconstruction.

4 Relative actuator gain calibration in step 12 (locked ITF)

4.1 Measurement principle

Using groups of lines injected on the different mirrors on the locked ITF, one can fit the optical gain of the cavities within a few assumptions. The optical gains being inversely proportional to the actuator gain, it is a way to measure the shape of the actuation TF moduli. The configuration of the detector as well as the method being completely different from the free swinging Michelson data described in previous section, the comparison of both results can be used to estimate systematic errors on the shape of the actuator responses. This method also allow to measure the moduli up to higher frequencies ($\sim$ 2 kHz) than the direct measurements ($\sim$ 600 Hz) that can thus be extrapolated.

Groups of four lines are injected on the end, BS and PR mirrors at frequencies f_i (i=1..4) respectively, the f_i being within 2 Hz from the frequency f_j. The dark fringe signal FFT is then measured. It can also be derived from other parameters:

$$Pr\_B1(f) = \sum_{m=1}^{m=4} \Delta L_m(f) \times O_m^{\text{cavity}_m}(f) \tag{13}$$

$$\tag{14}$$

The mirror movement amplitude can be estimated from the previously measured actuation TF G_m^{actuator} and the actuator input signals $zCorr_m$, taking into account the pendulum response TF_{pendulum}:

$$\Delta L_m(f) = zCorr_m(f) \times G_m^{\text{actuator}}(f) \times TF_{\text{pendulum}}(f) \tag{15}$$

The set of four equations obtained at the frequencies f_i can be solved to derive the optical gain at the frequency f_j. Some assumptions are used in this calculation[11]:

- simple cavity filtering $O_m^{\text{cavity}_m}(f)$ with a pole at 500 Hz,
- simple pendulum response: $TF_{\text{pendulum}}(f) \propto \left(\frac{f_0}{f}\right)^2$, with $f_0 = 0.6$ Hz,
- shape of the actuation TF moduli: $G_m^{\text{actuator}}(f)$.

The optical gain can thus be estimated as function of the frequency since N different groups of lines are injected close to the frequencies f_j (j=1..N).

4.2 Relative actuation gain measurements

15 minutes of data were taken on March, 7th 2007 (logbook entry 15496) with the ITF locked in step 12 (adjusting mode). Twenty lines were injected on every towers NE, WE, NI, WI, BS and PR, from 6 Hz to 800 Hz. All towers were in LN mode.

The optical gains relative their the value at 356 Hz have been estimated as shown above. The figure 19 show their dependency with frequency for every towers assuming a flat BS actuation TF, and TF with poles and zeros as described in table 8 for the arm actuation as well as for PR. The flatness of the optical gains as function of frequency above $\sim$ 40 Hz for the BS and arm mirrors indicates that the actuation TF parametrisation in LN mode is well described by a pole and a zero as seen in HP mode. Contrary to the HP gain, no discrepancy with the parametrisation is seen above 300 Hz in LN mode. The PR actuation TF must have a different shape than the other mirrors at high frequency where the optical gains increase.

[11] The readout response is flat within 2% since the calibration of the compression filters of the demodulation boards. See logbook entry 15067

Below $\sim$ 40 Hz, the mirror control signals are reallocated to the marionnette. Since the marionnette response is not calibrated nor used in this analysis, the optical gain below *sim*40 Hz cannnot be estimated properly.

The figure 20 shows the permanent calibration line subtraction. The optical gains are fitted using the 359 Hz line

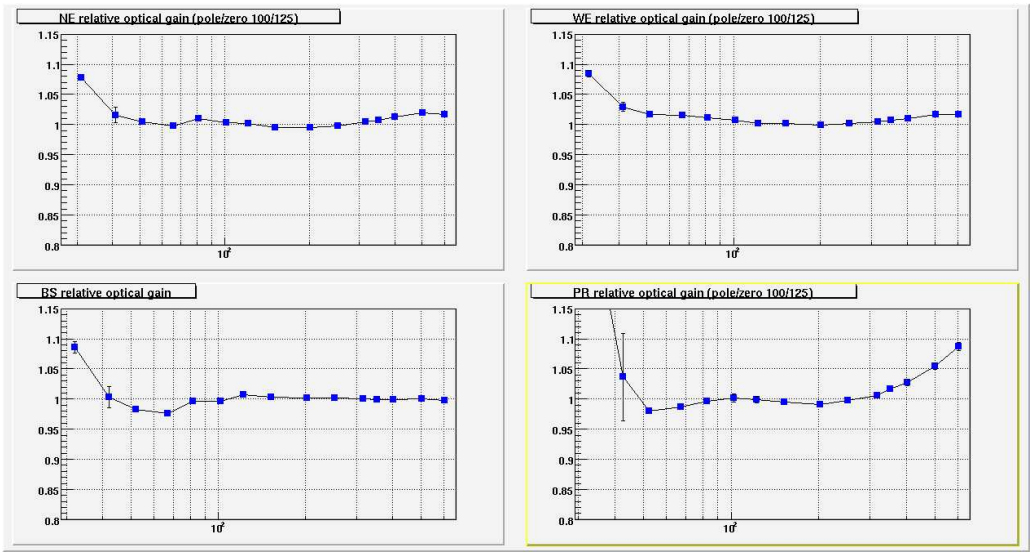

Figure 19: ***Relative optical gain vs frequency****, estimated assuming for the actuation TF in LN mode the same frequency dependence as parametrized in HP mode.*

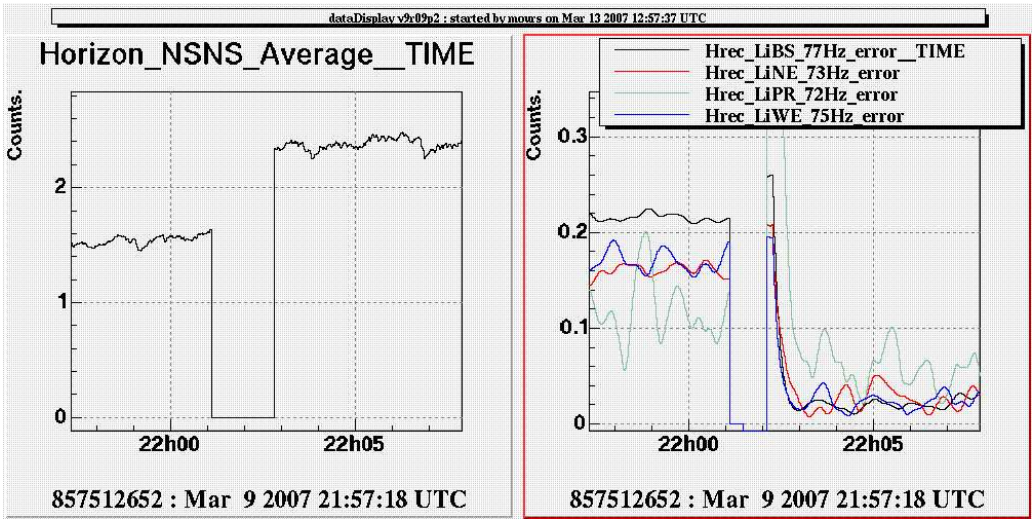

Figure 20: ***Residual of the line subtraction with locked ITF****, assuming flat actuation gain first, and assuming the same frequency dependence as parametrized in HP mode after.*

A Some hardware modifications

- Before November, 23rd, 2006, the clipping values of NE and WE were changed from 6 and 4 V respectively to 2 V. (Vincenzo Datilio, logbook entries 14217)
- November, 29th, 2006, replacement of the deficient DAC in the actuation part of the WE LN coil driver channel (logbook entry ??). See Fig. 21 and 22.
- Before **??????**November, 2006, the emphasis filter in the NI (?) mirror was used only in LN mode (Dominique Huet).
- Before **??????**November, 2006, no emphasis filter was used in the WI (?) DSP (Dominique Huet).
- January, 2nd-3rd 2007, add protection resistors (39Ω) on the coil drivers of NE, WE, NI, WI and BS. Update the DSP digital gain to 4.7 in the NI and WI DSPs, as well as in the left and right coils of NE and WE DSPs. (Vincenzo Datilio, logbook entries 14609, 14620)
- February, 7th 2007, improve the compression/de-compression filter compensation on the B1 photodiodes demodulation board. Then compensation being then within 2% (Edwige Tournefier, Alain Masserot, logbook entry 15067).
- March 2007, Sc* channels for coil currents removed on end mirrors. Keep only Ca* channels (Alain Masserot).
- end March 2007, use the LAPP ADC on the Ca coil current channels on the BS coil driver (Dominique Huet).

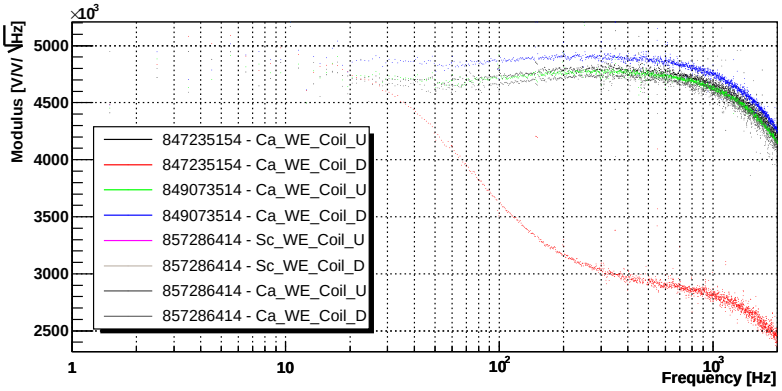

Figure 21: ***TF modulus of the WE coil current over*** *zCorr* ***in LN mode*** *for both up and down coils at different times from November 11th, 2006 to March 7th, 2007. The red points are the measurements of the down coil with the DAC failure while the blue points are the same measurements with the new DAC. Only points with coherence higher than 99% are plotted.*

Need to add the plot for C7 data.

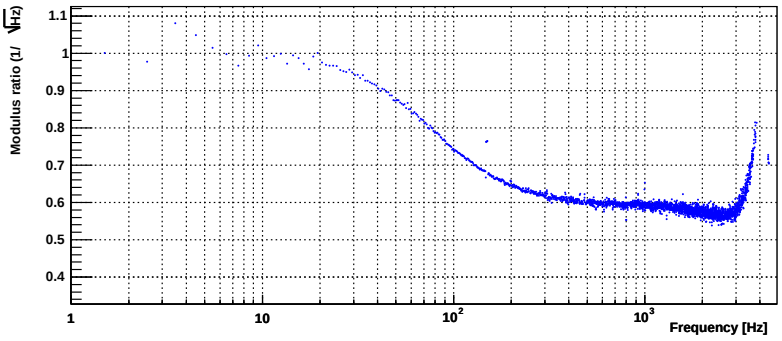

Figure 22: ***Ratio of the TF modulus of the WE down coil current over*** *zCorr* ***in LN mode:*** $\frac{\mathrm{TF(oldDAC)}}{\mathrm{TF(newDAC)}}$ *(GPS 847235154 and 849073514). Only points with coherence higher than 90% in both TFs are plotted.*

B Free Michelson ΔL reconstruction: $MinMax$ method

The principle of the method is discribed on page 3.2.2. The details of the algorithms are given here.

The parameters A, B and C are estimated from the minimum, maximum and average signals each time the angle $\Delta\Phi$ has moved by more than 2π since last estimation (or if more than 2 s of data was read for the very first computation).

They are then averaged using a sliding average that behaves as a low pass filter. The average value of A after the kth estimation, $< A >_k$ is computed from the previous average $< A >_{k-1}$ and the new value A_k:

$$< A >_k = (1-\epsilon)\times < A >_{k-1} + \epsilon \times A_k$$

where $\epsilon = 0.01$.

The value of $\Delta\Phi_i$ and ΔL_i are then estimated for every sample i from the last average values $< A >_k$, $< B >_k$ and $< C >_k$ as described on page 3.2.2. The ΔL_i values are saved into the frame at the same rate as the sampling of the photodiode signals Pr_B1p.

Two values of ΔL are computed, one using Pr_B1p_ACq and the other one using Pr_B1p_ACp (or the $B1$ signals).

The parameter average values $< A >_k>$, $< B >_k$ and $< C >_k$ are saved into the frame at the same rate as the photodiode signal with names $MinMax\_A\_ACq$, $MinMax\_B\_ACq$, $MinMax\_C\_ACq$ respectively (if they are computed with the quadrature signal ACq).

C Free Michelson ΔL reconstruction: *Ellipse* method

The *Ellipse* method is used to estimate the mirror displacement in free Michelson configuration as described in section 3.2. The details of the algorithm are given here. It is based on the fact that the phase (Pr_B1p_ACp) or quadrature (Pr_B1p_ACq) photodiode signals plotted as function of the DC signal has an elliptic shape.

C.1 General algorithm

Two values of ΔL are estimated from both the phase and quadrature signals. The following exemples are given for the quadrature signal.

The kth averaged ellipse centre position (X_0^k, Y_0^k) and axis width ratio σ_X^k/σ_Y^k are estimated from the DC and ACq. Then the angle $\Delta\Phi_i$ of the following samples i are estimated from the relation:

$$\cos\Delta\Phi_i = \frac{DC_i - X_0^k}{\sigma_X^k} \quad (16)$$

$$\sin\Delta\Phi_i = \frac{ACq_i - Y_0^k}{\sigma_Y^k} \quad (17)$$

$$(18)$$

The current ellipse parameters x_0^k, y_0^k, σ_x^k, σ_y^k are estimated using the method described below from buffered samples of DC and ACq signals every time that the current $\Delta\Phi_k$ differs by more than 2π from its value when the last ellipse $\Delta\Phi_{k-1}$ was fitted and that the number of samples in the buffer is more than 20 (the first ellipse is computed using 1 000 samples in the buffer). They are then average using a sliding averaged defined as:

$$X_0^k = (1-\epsilon) \times X_0^{k-1} + \epsilon \times x_0^k$$

for the X_0^k parameter for exemple, with $\epsilon = 0.001$

The estimated values of ΔL as well as the estimated values of the averaged ellipse parameters are saved into the frame at the same rate as the photodiode signals.

C.2 Ellipse fitting method algorithm

A numerically stable non -iterative algorithm for fitting an ellipse to a set of data points is described in [8]. It has been added in the Cali module using the matrix objects from ROOT in CaliCommon, under the name HalirFlusserMethod.

Ellipse fitting method description - The method takes as arguments a set of N coordinates (x_i, y_i), $i \subset (1, N)$. The ellipse is described by an implicit second order polynomial:

$$F(x,y) = ax^2 + bxy + cy2 + dx + ey + f = 0$$

and the six unknown ellipse parameters are (a, b, c, d, e, f).

From the data, two $N \times 3$ matrixes are built:

$$D_1 = \begin{pmatrix} x_1^2 & x_1y_1 & y_1^2 \\ . & . & . \\ . & . & . \\ x_i^2 & x_iy_i & y_i^2 \\ . & . & . \\ . & . & . \\ x_N^2 & x_Ny_N & y_N^2 \end{pmatrix}$$

$$D_2 = \begin{pmatrix} x_1 & y_1 & 1 \\ . & . & . \\ . & . & . \\ x_i & y_i & 1 \\ . & . & . \\ . & . & . \\ x_N & y_N & 1 \end{pmatrix}$$

Then, four 3×3 matrixes are defined:

$$S_1 = D_1^T \times D_1 \quad (19)$$
$$S_2 = D_1^T \times D_2 \quad (20)$$
$$S_3 = D_2^T \times D_2 \quad (21)$$
$$(22)$$

and

$$C_1 = \begin{pmatrix} 0 & 0 & 1/2 \\ 0 & -1 & 0 \\ 1/2 & 0 & 0 \end{pmatrix}$$

From these objects, one computes the 3×3 matrix M:

$$M = C_1^{-1} (S_1 - S_2 S_3^{-1} S_2^T)$$

The three eigenvectors v_j of M are then calculated. One of these vectors, called $a_1 = (a, b, c)$, represents the ellipse parameters. To choose among them, one estimated the number $s = a_1^T C_1 a_1$ and select the vector a_1 with the more little positive s value. The other ellipse parameters are then calculated as:

$$a_2 = -S_3^{-1} S_2^T a_1 = (d, e, f)$$

At this point, the six parameters (a, b, c, d, e, f) are fitted.

As the fitted ellipse of the AC vs DC signals has its main axis parallel to x and y:

$$\frac{(x - x_0)^2}{\sigma_x^2} + \frac{(y - y_0)^2}{\sigma_y^2} = 1$$

one can deduce from the parameters the ellipse center coordinates (x_0, y_0) and the normalized axis lengths (σ_x, σ_y):

$$\sigma_x^2 = \frac{1}{a} \quad (23)$$
$$\sigma_y^2 = \frac{1}{c} \quad (24)$$
$$x_0 = -\frac{\sigma_x^2 \times d}{2} \quad (25)$$
$$y_0 = -\frac{\sigma_y^2 \times e}{2} \quad (26)$$

These four parameters are returned by the HalirFlusserMethod function and used to average the ellipse parameters over time and to compute the $\Delta\Phi$ angle of the following data points.

The resolution of the ellipse centre and sigma reconstruction has been estimated and is better than 1%. This part still need to be written.

References

[1] Fabrice Beauville, PhD manuscript, 2005 (LAPP-T-2005-07).

[2] Olivier Véziant, PhD manuscript, 2003.

[3] Pendulum mechanical response ???

[4] R. Flaminio, F. Marion, B. Mours, O. Véziant, VIRGO note (2002) VIR-NOT-LAP-1390-204

[5] A. Gennai, VIRGO note (2004) VIR-SPE-PIS-4900-121

[6] P. Puppo, P. Rapagnani, VIRGO note (2005) VIR-NOT-ROM-1390-311

[7] P. Puppo, private discussion, 2007

[8] R. Halir and J. Flusser, *Numerically stable direct least squares fitting of ellipses*, in Skala, V(ed.)Proc.Int.Conf. in Central Europe on Computer Graphics, Vizualisation and Interactive Digital Media, 125–132 (1998).